Available online at www.sciencedirect.com
SCIENCE DIRECT®
International Journal of Thermal Sciences 43 (2004) 1181–1186
International Journal of Thermal Sciences
www.elsevier.com/locate/ijts

Maximal heat transfer density: Plates with multiple lengths in forced convection

T. Bello-Ochende, A. Bejan *

Department of Mechanical Engineering and Materials Science, Duke University, Box 90300, Durham, NC 27708-0300, USA

Received 8 January 2004; received in revised form 28 April 2004; accepted 5 May 2004

Available online 11 September 2004

Abstract

This paper shows that in a space filled with heat generating parallel plates and laminar forced convection, the heat transfer density can be increased beyond the level known for parallel plates with optimal spacing. The technique consists of inserting in every entrance region new generations of smaller plates, because smaller plates have thin boundary layers that fit in the unused (isothermal) entrance flow. This technique can be repeated several times, and the result is a sequence of multi-scale flow structures that have progressively higher heat transfer densities. The work consists of numerical simulations in a large number of flow configurations, one differing slightly from the next. The complete optimized architecture and performance of structures with one, two and three plate length scales are reported. Diminishing returns are observed as the number of length scales increases. This method can be used to develop multi-scale nonuniform flow structures for heat exchangers and cooled electronic packages.

Keywords: Constructal design; Optimal spacings; Multi-scale structures; Pressure drop number; Optimized complexity

1. Introduction

Compactness and miniaturization are driven by the need to install more and more heat transfer into a given volume. The figure of merit is heat transfer density. A recent trend in heat transfer research has been the focus on the generation of optimal flow architecture, as a mechanism by which the system achieves its maximal density objective under constraints [1]. The strategy is to endow the flow configuration with the freedom to morph, and to examine systematically many of the eligible design configurations en route to the best. Strategy and systematic search mean that architectural features that have been found to be beneficial in the past can be refined and incorporated in more complex systems of the present.

One class of flow features that aid the achievement of high heat transfer density are the optimal spacings that have been reported for natural convection [2–4] and forced convection [5,6]. The progress in this area has been reviewed in [1,7]: Optimal spacings have been determined for parallel plates channels, cylinders in cross-flow, staggered parallel plates, and pin fin arrays with impinging flow. In each configuration, the optimal spacing is a single length scale that is distributed throughout the available volume.

The optimal spacing idea was taken theoretically one step further in [8], where the flow structure had not one but several optimal length scales. These were distributed nonuniformly through the flow space—more numerous and smaller in the entrance region of the available volume, because there the boundary layers were thinner and more plates could be fitted together optimally.

In this paper, we evaluate this design approach numerically, by considering forced convection cooling of a volume filled by parallel plates that generate heat. The flow and heat transfer are simulated numerically for a wide variety of flow configurations. Each numerical simulation shows that the entrance region of every parallel-plates channel has a core of unused (isothermal) fluid. In this wedge-shaped region we

* Corresponding author.
E-mail address: dalford@duke.edu (A. Bejan).

1290-0729/$ – see front matter
doi:10.1016/j.ijthermalsci.2004.05.002

Nomenclature

Be	pressure drop number, Eq. (11)	q''	heat flux ..... $W\cdot m^{-1}\cdot K^{-1}$
D_0	spacing between L_0 plates ..... m	T	temperature ..... K
D_1	spacing between the L_0 and L_1 plates when the L_1 plate is inserted ..... m	T_w	wall temperature ..... K
D_2	spacing between the L_1 and L_2 plates when the L_1 and L_2 plates are inserted ..... m	T_∞	inlet temperature ..... K
k	thermal conductivity ..... $W\cdot m^{-1}\cdot K^{-1}$	u, v	velocity components ..... $m\cdot s^{-1}$
L_0	flow length ..... m	x, y	cartesian coordinates ..... m
L_1	flow length of the first insert ..... m	*Greek symbols*	
L_2	flow length of the second insert ..... m	α	thermal diffusivity ..... $m^2\cdot s^{-1}$
P	pressure ..... P	ΔP	pressure difference ..... Pa
Pr	Prandtl number	μ	viscosity ..... $kg\cdot sm^{-1}$
q	total heat transfer ..... W	ν	kinematic viscosity ..... $m^2\cdot s^{-1}$
$\tilde{q}$	dimensionless heat transfer density, Eq. (15)	ρ	density ..... $kg\cdot m^{-3}$
$\tilde{q}_0$	dimensionless heat transfer density with no plate inserts	*Superscripts*	
$\tilde{q}_1$	dimensionless heat transfer density with L_1 inserts	m	maximum
$\tilde{q}_2$	dimensionless heat transfer density with L_1 and L_2 inserts	opt	optimum
q'	heat transfer rate per unit length .. $W\cdot m^{-1}\cdot K^{-1}$	w	wall
		Superscript	
		$\tilde{}$	dimensionless variables, Eq. (5)

insert progressively smaller heat generating plates, and then we optimize the multi-scale assembly. The maximization of heat transfer density is pursued geometrically, by varying more and more degrees of freedom. The result is a class of progressively better flow structures with multiple length scales that are distributed nonuniformly through the flow system.

2. Model

The plates geometry is shown in Fig. 1. The longest plates have the length L_0, and the spacing between them is D_0. Shorter plates with the lengths L_1, L_2, ..., and thickness t are inserted between the long plates. A related geometry has been studied numerically in [9]. The flow through the plates is laminar forced convection driven by the imposed pressure difference ΔP. The objective of this study is to determine the optimal lengths of the plates that can be inserted in this channel such that the heat transfer rate density is maximized.

In the model shown in Fig. 1, the flow is assumed to be steady, laminar, incompressible and two-dimensional, and all the thermophysical properties are constant. The symmetry of the configuration in Fig. 1 allows us to study only half of the flow structure, as shown in Fig. 1(b). The steady state conservation equations for mass, momentum, and energy are

$$\frac{\partial u}{\partial x}+\frac{\partial v}{\partial y}=0 \tag{1}$$

$$u\frac{\partial u}{\partial x}+v\frac{\partial u}{\partial y}=-\frac{1}{\rho}\frac{\partial P}{\partial x}+\nu\nabla^2 u \tag{2}$$

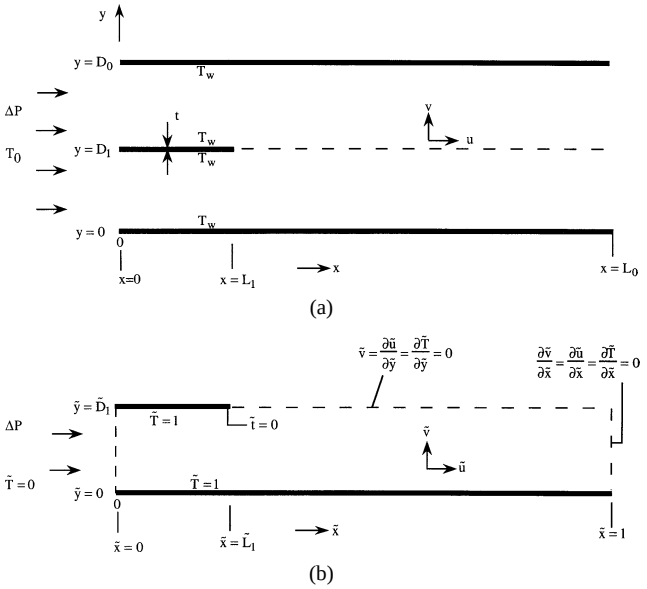

Fig. 1. The physical domain, computational domain and boundary conditions.

$$u\frac{\partial v}{\partial x}+v\frac{\partial v}{\partial y}=-\frac{1}{\rho}\frac{\partial P}{\partial x}+\nu\nabla^2 v \tag{3}$$

$$u\frac{\partial T}{\partial x}+v\frac{\partial T}{\partial y}=\alpha\nabla^2 T \tag{4}$$

where $\nabla^2=\partial^2/\partial x^2+\partial^2/\partial y^2$. The computational domain is shown in Fig. 1(b). The horizontal and vertical velocity components are u and v. The above equations were nondimensionalized by using the following variables

$$\left(\tilde{x}, \tilde{y}, \widetilde{L}_1, \widetilde{L}_2, \widetilde{D}_0, \widetilde{D}_1, \widetilde{D}_2, \tilde{t}\right) = (x, y, L_1, L_2, D_0, D_1, D_2, t)/L_0 \tag{5}$$

$$\widetilde{T} = \frac{T - T_\infty}{T_w - T_\infty}$$

$$\widetilde{P} = \frac{P}{\Delta P}, \qquad (\tilde{u}, \tilde{v}) = \frac{(u, v)}{\Delta P L_0/\mu} \tag{6}$$

The resulting governing equations are

$$\frac{\partial \tilde{u}}{\partial \tilde{x}} + \frac{\partial \tilde{v}}{\partial \tilde{y}} = 0 \tag{7}$$

$$\frac{Be}{Pr}\left(\tilde{u}\frac{\partial \tilde{u}}{\partial \tilde{x}} + \tilde{v}\frac{\partial \tilde{u}}{\partial \tilde{y}}\right) = -\frac{\partial \widetilde{P}}{\partial \tilde{x}} + \nabla^2 \tilde{u} \tag{8}$$

$$\frac{Be}{Pr}\left(\tilde{u}\frac{\partial \tilde{v}}{\partial \tilde{x}} + \tilde{v}\frac{\partial \tilde{v}}{\partial \tilde{y}}\right) = -\frac{\partial \widetilde{P}}{\partial \tilde{y}} + \nabla^2 \tilde{v} \tag{9}$$

$$Be\left(\tilde{u}\frac{\partial \widetilde{T}}{\partial \tilde{x}} + \tilde{v}\frac{\partial \widetilde{T}}{\partial \tilde{y}}\right) = \nabla^2 \widetilde{T} \tag{10}$$

where the Prandtl number is ν/α, and Be is the dimensionless pressure drop number [6,10]

$$Be = \frac{\Delta P L_0^2}{\alpha \mu} \tag{11}$$

The boundary conditions for fluid flow are: $\widetilde{P} = 1$, $\tilde{v} = 0$ and $\partial \tilde{u}/\partial \tilde{x} = 0$ at the inlet of the computational domain ($\tilde{x} = 0$); $\widetilde{P} = 0$ and $\partial(\tilde{u}, \tilde{v})/\partial \tilde{x} = 0$ at the exit ($\tilde{x} = 1$); no slip and no penetration on the plate surfaces; and $\tilde{v} = 0$ and $\partial \tilde{u}/\partial \tilde{y} = 0$ on the plane of symmetry. The temperature boundary conditions are: $\widetilde{T} = 1$ on the blades surfaces, and $\widetilde{T} = 0$ on the inlet plane of the computational domain. The exit plane and the plane of symmetry are modeled as adiabatic.

We are interested in the geometric arrangement for which the overall heat transfer rate is maximum. The local heat flux from the horizontal plate for a case where the number of inserted plates is equal to 2, is

$$q'' = k\left(-\frac{\partial T}{\partial y}\right)_{y=0} + k\left(\frac{\partial T}{\partial y}\right)_{y=(D_2)^-} + k\left(-\frac{\partial T}{\partial y}\right)_{y=(D_2)^+} + k\left(\frac{\partial T}{\partial y}\right)_{y=(D_1)^-} \tag{12}$$

This flux is integrated over the total heat transfer surfaces to obtain the total heat transfer from the $D_0 L_0$ space,

$$q' = k\int_0^{L_0}\left(-\frac{\partial T}{\partial y}\right)_{y=0} \mathrm{d}x + k\int_0^{L_2}\left(\frac{\partial T}{\partial y}\right)_{y=(D_2)^-} \mathrm{d}x + k\int_0^{L_2}\left(-\frac{\partial T}{\partial y}\right)_{y=(D_2)^+} \mathrm{d}x + k\int_0^{L_1}\left(\frac{\partial T}{\partial y}\right)_{y=(D_1)^-} \mathrm{d}x \tag{13}$$

The dimensionless total heat transfer rate is

$$\tilde{q}' = \frac{q'}{k(T_w - T_\infty)} = \int_0^1\left(-\frac{\partial \widetilde{T}}{\partial \tilde{y}}\right)_{\tilde{y}=0} \mathrm{d}\tilde{x} + \int_0^{\widetilde{L}_2}\left(\frac{\partial \widetilde{T}}{\partial \tilde{y}}\right)_{\tilde{y}=(\widetilde{D}_2)^-} \mathrm{d}\tilde{x} + \int_0^{\widetilde{L}_2}\left(-\frac{\partial \widetilde{T}}{\partial \tilde{y}}\right)_{\tilde{y}=(\widetilde{D}_2)^+} \mathrm{d}\tilde{x} + \int_0^{\widetilde{L}_1}\left(\frac{\partial \widetilde{T}}{\partial \tilde{y}}\right)_{\tilde{y}=(\widetilde{D}_1)^-} \mathrm{d}\tilde{x} \tag{14}$$

The total dimensionless heat transfer rate density is

$$\tilde{q} = \frac{\tilde{q}'}{\widetilde{D}_0} = \frac{q'}{k(T_w - T_\infty)\widetilde{D}_0} \tag{15}$$

The heat transfer rate density was calculated based on the total heat transfer from all the plates, divided by the total volume. This quantity is the heat transfer density, which is proportional to the ratio q'/D_0, cf. Eq. (15).

3. Numerical method

Eqs. (8)–(10) were solved using a finite element code [11] with quadrilateral elements and biquadratic interpolation functions. For more details see [12]. The nonlinear equations resulting from the Galerkin finite-element discretization of Eqs. (8)–(10) were solved using successive substitution followed by the quasi-Newton method. As convergence criteria we used

$$\frac{\|u^{(k)} - u^{(k-1)}\|}{\|u^k\|} \leqslant 10^{-4} \quad \text{and} \quad \frac{\|R(u^{(k)})\|}{\|R_0\|} \leqslant 10^{-4} \tag{16}$$

where $\boldsymbol{R}(\boldsymbol{u})$ is the residual vector, $\boldsymbol{u}$ is the complete solution vector, k is the iteration counter, and $\|\cdot\|$ is the Euclidian norm. The grid was nonuniform in both $\tilde{x}$ and $\tilde{y}$ directions. The grid was double graded in the $\tilde{y}$ direction so as to put more nodes near the plate surfaces to capture more accurately the behavior in the boundary layers. The grid varied from one geometric configuration to another. Grid refinement tests performed in the range $10^5 \leqslant Be \leqslant 10^8$ and $Pr = 1$, indicated that the solutions were insensitive to further grid doubling in $\tilde{x}$ and $\tilde{y}$ when 400 nodes per L_0 were used in both $\tilde{x}$ and $\tilde{y}$ directions. Table 1 shows how grid independence was achieved. To validate the numerical scheme

Table 1
Grid refinement test for $\widetilde{D} = 0.06$, $Be = 10^6$ and $Pr = 1$

Number of nodes per L_0 in $\tilde{x}$ and $\tilde{y}$ directions	$\tilde{q}$	$\left\lvert\frac{\tilde{q}^i - \tilde{q}^{i+1}}{\tilde{q}^i}\right\rvert$
100	512.08	–
200	515.42	0.0065
400	518.50	0.0058
800	520.67	0.0041

further, the scheme was used to generate results for the optimal spacing between parallel plates with forced convection. These results were then compared with results available in the literature [5], and the agreement was found to be very good.

The optimized results reported in this paper are mesh independent. Independence was achieved by increasing the number of nodes per L_0 during simulations in the vicinity of the optimal spacing. The number of nodes per L_0 was increased until it had no effect on the maximized $\tilde{q}$ value. This ensured that each optimized flow architecture is independent of the grid fineness. The algorithm used for determining the optimal dimensions (L_i, D_i) consisted of nested loops, such that the $\tilde{q}$ value was calculated for all possible combinations of (L_i, D_i) in the vicinity of the architecture with the maximum $\tilde{q}$ value.

4. Numerical results

In this section we present the numerical results for the optimal spacing $\widetilde{D}_{0,\mathrm{opt}}$, and the corresponding maximum heat transfer density $\tilde{q}_m$. We also report the optimal length scales when new plates are inserted in the structure $\widetilde{D}_0 L_0$, leading to new optimal spacings and revised estimates of the maximum heat transfer density. The numerical optimization was performed in the range $10^5 \leqslant Be \leqslant 10^8$ and $Pr = 1$. The thickness of the $\widetilde{L}_2$ plate was set at $\tilde{t} = 10^{-4}$.

The optimization of the multiscale structure has several degrees of freedom. First, we determined the optimal spacing and maximal $\tilde{q}$ when $\widetilde{L}_1 = 0$, i.e., there are no inserts in the channel formed between two L_0 plates. The optimization of the spacing $\widetilde{D}_0$ is illustrated in Fig. 2.

Next, we inserted a $\widetilde{L}_1$-long plate as shown in Fig. 1, and optimized simultaneously the two length scales of the configuration, $\widetilde{L}_1$ and the spacing $\widetilde{D}_1$. This work is illustrated in Fig. 3. Because in this case the computational domain is symmetric about $\tilde{y} = \widetilde{D}_1$, we were able to set $\tilde{t} = 0$ for the thickness of the $\widetilde{L}_1$ plate. Note that the spacing between the L_0 plates becomes $\widetilde{D}_0 = 2\widetilde{D}_{1,\mathrm{opt}}$, and that this value is slightly larger than the $\widetilde{D}_{0,\mathrm{opt}}$ value found when the L_1 plate is absent. In other words, the insertion of a smaller plate at the entrance of a channel enlarges the optimal spacing of that channel.

In the final step of this sequence of increasingly more complex structures, we inserted an even smaller L_2 plate in the entrance formed between the L_0 and L_1 plates. As shown in Fig. 4, we optimized the dimensions $\widetilde{L}_2$ and $\widetilde{D}_2$ while holding $\widetilde{L}_{1,\mathrm{opt}}$ fixed at the value determined previously (Fig. 3). In this case the spacing between the $\widetilde{L}_0$ plates becomes $\widetilde{D}_0 = 2\widetilde{D}_{1,\mathrm{opt}} = 4\widetilde{D}_{2,\mathrm{opt}}$. The thickness of the $\widetilde{L}_2$ plate was again set at $\tilde{t} = 10^{-4}$. Fig. 5 shows that such a thickness is small enough so that the maximized $\tilde{q}$ is insensitive to changes in $\tilde{t}$. We have performed the same plate-thickness sensitivity study for $\mathrm{Be} = 10^6$, and arrived at the same conclusion: $\tilde{t} = 10^{-4}$ is small enough so that its effect on the optimized plate lengths and spacings is negligible.

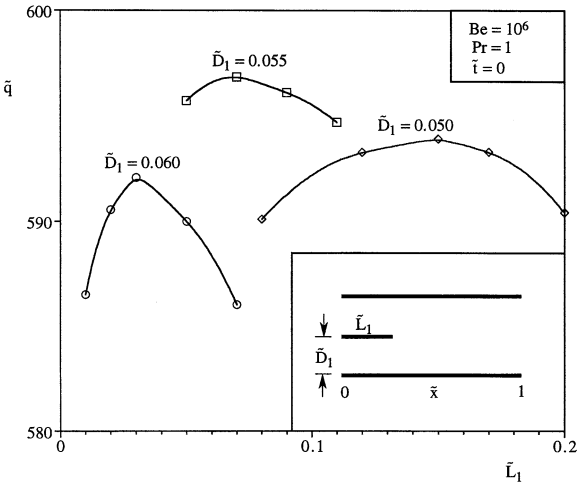

Fig. 3. The effect of the length $\widetilde{L}_1$ on the dimensionless total heat transfer density for $Be = 10^6$.

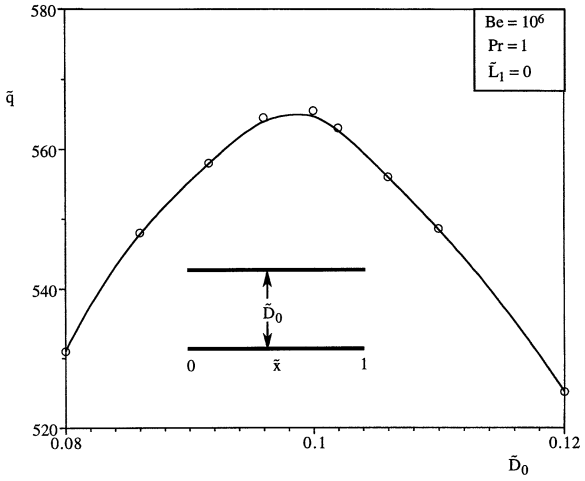

Fig. 2. The effect of plate spacing $\widetilde{D}$, on the dimensionless total heat transfer density in the absence of plate inserts.

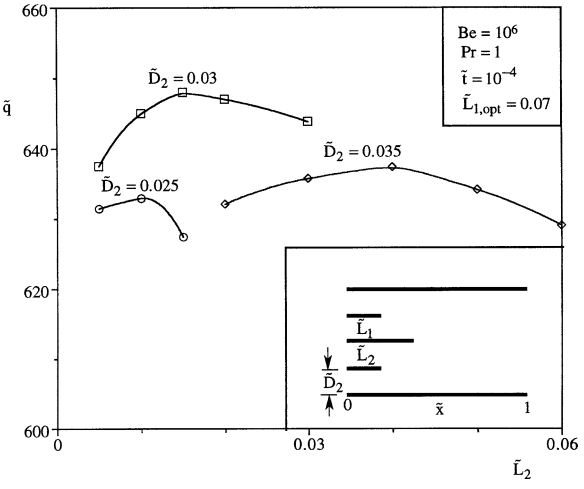

Fig. 4. The effect of the length $\widetilde{L}_2$ on the dimensionless total heat transfer density for $Be = 10^6$ by holding $\widetilde{L}_{1,\mathrm{opt}}$ fixed.

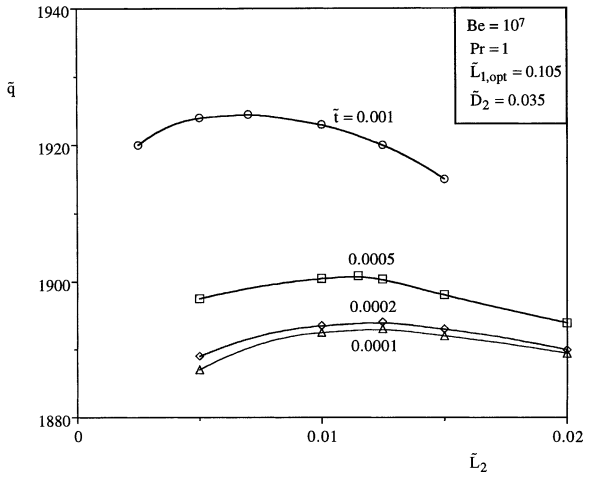

Fig. 5. The effect of the plate thickness on the dimensionless maximum total heat transfer rate density and $\widetilde{L}_2$.

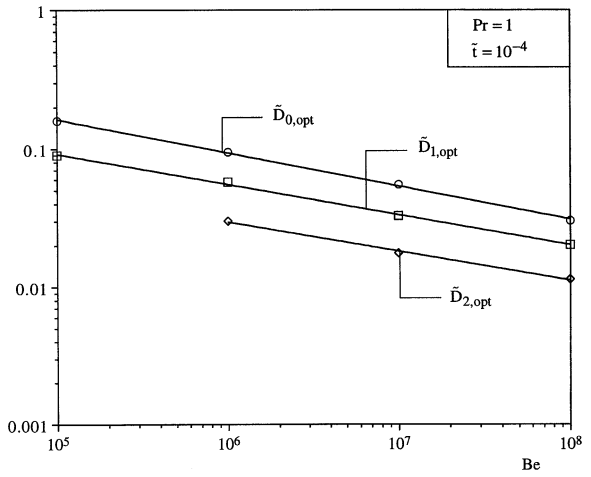

Fig. 6. The effect of the pressure drop number on the optimized spacings.

The stepwise increase in the largest spacing ($\widetilde{D}_0$, $\widetilde{D}_1$, $\widetilde{D}_2, \ldots$) is summarized in Fig. 6. The optimized spacing between the L_0 plates is now greater than when the L_2 plate was absent.

The procedure stated above was repeated for several *Be* values in the range $10^5 \leqslant Be \leqslant 10^8$ and $Pr = 1$. The results are shown in Figs. 6–8. Fig. 6 shows the behavior of the optimal spacings, $(\widetilde{D}_0, \widetilde{D}_1, \widetilde{D}_2)_{\text{opt}}$. The optimal spacing decreased as the dimensionless pressure drop increases. The ratios $\widetilde{D}_{0,\text{opt}}/\widetilde{D}_{1,\text{opt}}$ and $\widetilde{D}_{1,\text{opt}}/\widetilde{D}_{2,\text{opt}}$ are nearly constant and equal to 1.83 and 1.76, respectively. As shown in [8], the theoretical ratio of successive spacings is 2. The numerically derived ratios are not exactly equal to 2 because the spacing between the $\widetilde{L}_0$ plates increases slightly when a new (smaller) plate is inserted and the spacings and lengths are optimized.

Fig. 7 shows the behavior of the optimal length scales $(\widetilde{L}_{1,\text{opt}}, \widetilde{L}_{2,\text{opt}})$. The optimal length scales increase as the dimensionless pressure drop number increases. The ratio $L_{2,\text{opt}}/L_{1,\text{opt}}$ is nearly constant and equal to 0.15. In the analytical treatment of the same problem [8], the optimal ratio

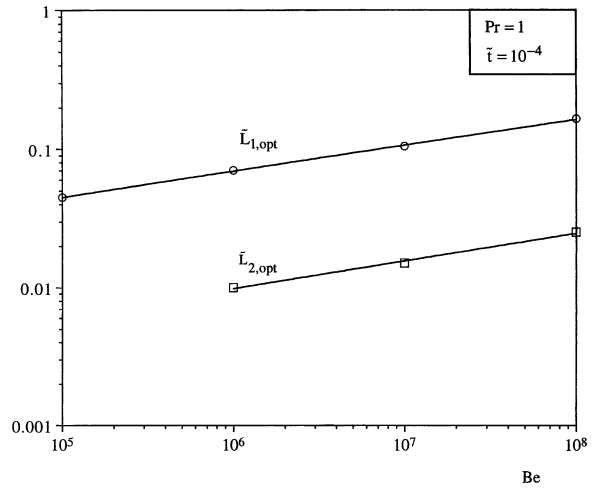

Fig. 7. The effect of the pressure drop number on the optimized length scales.

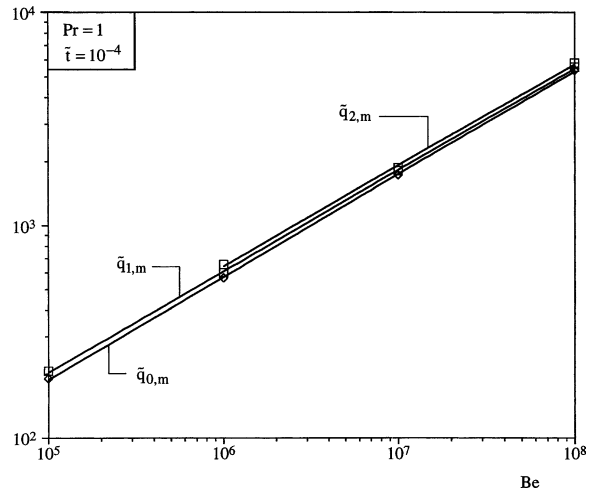

Fig. 8. The effect of the pressure drop number and the number of length scales on the dimensionless maximum total heat transfer density.

was $L_2/L_1 = 0.25$, which agrees with Fig. 7 in an order of magnitude sense. Furthermore, in [8] it was pointed out that the theoretical ratio $L_2/L_1 = 0.25$ is at best an approximation because it is based on the assumption that the insertion of each new (smaller) plate has a negligible effect on the boundary layers coating the older (longer) plates. Indeed, the present work shows that this assumption is indeed an approximation, because each new plate insert affects the optimal spacing between existing plates. Because the optimal spacing is governed by the thicknesses of the boundary layers that merge at the end of each channel, this means that the insertion of a small plate in the entrance region influences the older boundary layers that continue downstream. The insertion of a small plate near the channel entrance has the effect of thickening the older boundary layers, and enlarging the optimal spacing between the older plates.

Fig. 8 shows the effect of *Be* on the maximal heat transfer rate density for several combinations of length scales. The maximal heat transfer rate density increases as the number

Table 2
Comparison between the numerical and analytical results for the maximized heat transfer rate density of the multi-scale flow construct

m	$\tilde{q}/Be^{1/2}$	
	Analytical [8]	Numerical, Fig. 8
0	0.36	0.558
1	0.44	0.593
2	0.51	0.606

of plates increases. The effect becomes less noticeable when the number of length scales is increased to three. An optimal length $\widetilde{L}_2$ was not found when $Be < 10^6$.

Fig. 8 also shows that the maximized heat transfer rate density increases in proportion with $Be^{1/2}$. This confirms the analytical result [8], which can be rewritten in the notation employed in this paper:

$$\tilde{q}_{[8]} = 0.36Be^{1/2}\left(1+\frac{m}{2}\right)^{1/2} \tag{17}$$

Parameter m is the number of new (inserted) plate lengths, for example, $m = 2$ in Fig. 4. The prediction (17) is that the heat transfer rate density increases in progressively smaller steps as the number of length scales increases. This is confirmed by the numerical results shown in Fig. 8. Table 2 shows that the numerical $\tilde{q}_m$ results are relatively less sensitive than $\tilde{q}_{[8]}$ to increasing m.

5. Conclusions

In this paper we illustrated the emergence of multi-scale forced convection flow structure for maximal heat transfer rate density installed in a fixed volume. This objective was achieved by inserting smaller plates in the entrance region formed between successive plates. This technique utilizes to the fullest the fluid surrounding the two tips of two neighboring plates, where the boundary layers are the thinnest. The number of plate length scales increases as the flow strength, or the driving pressure difference increases.

Optimal spacings were found numerically for structures with one, two and three length scales. Performance increases as complexity increases, but diminishing returns are also observed. The optimized spacings increase slightly with each new (smaller) plate that is inserted in the entrance region of each channel.

As the number of plates increases, the flow structure becomes less permeable and the flow rate decreases. At the same time, the total heat transfer rate density from the solid structure increases. It was found numerically that when the number of plates increases to three the increase in the heat transfer rate density becomes less noticeable, hence for the numerical computation the number of plates inserted in the flow structure was limited to two.

The number of plate length scales is limited by the validity of the boundary layer assumption. The smallest plate is the one where the plate length is comparable with the boundary layer thickness. This criterion was developed analytically in Refs. [8,13], where it was shown that the number (m) of plate length scales (in addition to L_0) is a slowly increasing function of Be. The $m(Be)$ function is reported on page 243 of Ref. [13], and in the range $10^4 < Be < 10^{11}$ is approximated by

$$m = 0.78(\log_{10} Be - 3) \tag{18}$$

For example, when $Be = 10^7$ we find that $m = 3.13$, which means that a structure with three inserts (L_1, L_2, L_3) is already too refined: the smallest plate (L_3) does not contribute much, because it is not swept by a distinct boundary layer. This reinforces the conclusion reached in the preceding paragraph.

The fundamental value of this study is that multi-scale flow structures are applicable to every sector of heat exchanger design. The novelty is the increase in heat transfer density, and the nonuniform distribution of length scales through the available space. This approach promises the development of new and unconventional internal flow structures for heat exchangers and cooled electronic packages.

References

[1] A. Bejan, Shape and Structure, from Engineering to Nature, Cambridge University Press, Cambridge, 2000.
[2] A. Bar-Cohen, W.M. Rohsenow, Thermally optimum spacing of vertical, natural convection cooled, parallel plates, J. Heat Transfer 106 (1984) 116–123.
[3] A. Bejan, Convection Heat Transfer, Wiley, New York, 1984, Chapter 4, Problem 11, p. 157.
[4] N.K. Anand, S.H. Kim, L.S. Fletcher, The effect of plate spacing on free convection between heated parallel plates, J. Heat Transfer 114 (1992) 515–518.
[5] A. Bejan, E. Sciubba, The optimal spacing for parallel plates cooled by forced convection, Internat. J. Heat Mass Transfer 35 (1992) 3259–3264.
[6] S. Petrescu, Comments on the optimal spacing of parallel plates cooled by forced convection, Internat. Heat Mass Transfer 37 (1994) 1283.
[7] S.J. Kim, S.W. Lee (Eds.), Air Cooling Technology for Electronic Equipment, CRC Press, Boca Raton, FL, 1996, Chapter 1.
[8] A. Bejan, Y. Fautrelle, Constructal multi-scale structure for maximal heat transfer density, Acta Mech. 163 (2003) 39–49.
[9] D. Naylor, D.J. Tarasuk, Natural convective heat transfer in a divided vertical channel: Part 1—Numerical study, J. Heat Transfer 115 (1993) 377–385.
[10] S. Bhattacharjee, W.L. Grosshandler, The formation of wall jet near a high temperature wall under microgravity environment, in: ASME HTD, vol. 96, 1988, pp. 711–716.
[11] FIDAP Theory Manual, Fluid Dynamics International, Evanston, IL, 1998, Revision 8.6.
[12] J.N. Reddy, D.K. Gartling, The Finite Element Method in Heat Transfer and Fluid Dynamics, CRC Press, Boca Raton, FL, 1994.
[13] A. Bejan, I. Dincer, S. Lorente, A.F. Miguel, A.H. Reis, Porous and Complex Flow Structures in Modern Technologies, Springer, New York, 2004.